RESEARCH PAPER

Hydrogen-assisted cracking in GMA welding of high-strength structural steels using the modified spray arc process

Thomas Schaupp [1] · Michael Rhode [1,2] · Hamza Yahyaoui [1] · Thomas Kannengiesser [1,2]

Abstract

High-strength structural steels are used in machine, steel, and crane construction with yield strength up to 960 MPa. However, welding of these steels requires profound knowledge of three factors in terms of avoidance of hydrogen-assisted cracking (HAC): the interaction of microstructure, local stress/strain, and local hydrogen concentration. In addition to the three main factors, the used arc process is also important for the performance of the welded joint. In the past, the conventional transitional arc process (Conv. A) was mainly used for welding of high-strength steel grades. In the past decade, the so-called modified spray arc process (Mod. SA) has been increasingly used for welding production. This modified process enables reduced seam opening angles with increased deposition rates compared with the Conv. A. Economic benefits of using this arc type are a reduction of necessary weld beads and required filler material. In the present study, the susceptibility to HAC in the heat-affected zone (HAZ) of the high-strength structural steel S960QL was investigated with the externally loaded implant test. For that purpose, both Conv. A and Mod. SA were used with same heat input at different deposition rates. Both conducted test series showed same embrittlement index "EI" of 0.21 at diffusible hydrogen concentrations of 1.3 to 1.6 ml/100 g of arc weld metal. The fracture occurred in the HAZ or in the weld metal (WM). However, the test series with Mod. SA showed a significant extension of the time to failure of several hours compared with tests carried out with Conv. A.

Keywords High-strength steel · GMA welding · Diffusible hydrogen · Implant test · Fractography

1 Introduction

To achieve the climate goals and the associated reductions in CO_2 emissions, modern steel constructions require the use of high-strength structural steels with yield strengths of 690 MPa and more. High-strength structural steel grades have been used for several decades, particularly in mobile crane construction [1, 2]. The field of application is currently being extended to wind turbine and bridge construction. Manufacturers offer numerous base and filler materials for this

purpose. However, the increasing strengths require significantly higher demands on the welding processing. In order to guarantee the mechanical properties of the base materials also in the welded joint, narrow process limits must be considered during the welding production [3–6]. Incorrect handling of the high-strength structural steels can lead to damage during production or operation. Above all, hydrogen-assisted cracking (HAC) poses a major hazard. These micro-cracks result from the critical interaction of local crack-critical microstructure, locally increased diffusible hydrogen concentration, and locally increased stress or strain in the weld metal or in the heat-affected zone (HAZ). Current standards for the welding processing of high-strength steels [4, 5, 7] contain recommendations to minimize the risk of HAC in welding processing.

In the last 2 to 3 decades, the alloying concepts for high-strength steel grades have been further developed [8]. Almost all manufacturers of base and filler materials use micro-alloying elements (V, Nb, and Ti). These different alloying concepts result in different welded microstructures and mechanical properties [9]. Micro-alloying elements also have a significant influence on hydrogen diffusion and trapping due

✉ Thomas Schaupp
   thomas.schaupp@bam.de

[1] Bundesanstalt für Materialforschung und -prüfung (BAM), Unter den Eichen 87, 12205 Berlin, Germany

[2] Otto-von-Guericke-University, Universitätsplatz 2, 39106 Magdeburg, Germany

to precipitations and different resulting grain size, which is reflected in low diffusion coefficients of hydrogen in steels [10–13]. Modern high-strength steels and their weld metals are therefore subjected to increased susceptibility to time-delayed HAC. Especially, welded microstructures of high-strength materials with yield strengths ≥ 960 MPa can be very susceptible to HAC at diffusible hydrogen concentrations of $H_D \geq 1$ ml/100 g [14, 15]. It is therefore essential to ensure hydrogen effusion during welding and thus, reduce H_D in the welded joint to a minimum to avoid HAC.

High-strength steels are conventionally joined by gas metal arc (GMA) welding in the working area of the transitional arc (Conv. A) between short arc and spray arc [16]. The development of modern inverter technique welding machines with high-frequency control has led to modified process control variants in recent years [17, 18]. These welding power sources are offered by different manufacturers as modified spray arc processes (Mod. SA). In comparison with the Conv. A, the Mod. SA allows a larger contact-tube-to-work distance (CTWD) at very short arc length, high plasma pressure, and high deposition rates. These characteristics lead to advantages such as reduction of weld seam opening angles and therefore, required filler material and welding time (see Fig. 1). In multi-layer welding of 20-mm-thick butt joints with V-groove of S960QL, the welding time could be reduced by a factor of approximately 3 to 4 (depending on heat input and interpass temperatures) by reducing the weld seam opening angle from 60 to 30° [19].

Investigations on butt joints with V-groove [19–21] showed that in weldments with Mod. SA and reduced weld seam opening angle, higher H_D can be present in the weld metal compared with weldments carried out with Conv. A with wider groove. At higher deposition rates and the associated higher welding currents with Mod. SA, more hydrogen can be dissociated in the arc and absorbed by the weld metal [20, 22]. Regardless of the arc process and seam configuration, the mean hydrogen concentrations in the weld metal were $H_D \geq 1$ ml/100 g for single-pass welds [20]. With a proper choice of heat input and interpass temperatures, H_D could be reduced during multi-layer welding [19, 21]. However, the

deeper weld penetration profile when using Mod. SA with higher deposition rate resulted in longer diffusion paths for hydrogen. Therefore, the required high cooling rates (low $t_{8/5}$-cooling times) can prevent enough hydrogen effusion during welding. For complete hydrogen effusion out of the weld metal and reduction of related HAC, a dehydrogenation heat treatment (DHT) directly from the welding heat with sufficient temperature and dwell time is recommended [19, 23, 24]. Also, the standard [4] refers to DHT after welding processing independent of the used arc process or seam configuration. Further procedures to reduce HAC are depending on the used materials and the restraint intensity of the welded component [5, 7].

To investigate HAC of high-strength steels, many test methods exist [25, 26]. These tests can be classified as self-restraint and externally loaded tests. In self-restraint tests, the required stresses result from residual stresses and restraint of shrinkage due to the geometry of the specimens. These tests are used, for example, to determine required preheat temperatures or heat inputs for avoiding HAC [27] or to determine the time of crack initiation [28, 29] in weld metal and HAZ. In externally loaded tests, mechanical stresses are applied by a loading device. The most common externally loaded test is the implant test [30]. This test is mainly used to study the HAC susceptibility of the HAZ. Examinations regarding HAC in the weld metal can only be carried out with enormous effort as specimens have to be manufactured of the weld metal. In many investigations, delayed cracking [31, 32] as well as the influence of H_D [33] and different types of base and filler materials [34, 35] on HAC susceptibility were analyzed. Recent research dealt with the influence of chemical composition or manufacturing process of base materials on HAC in the HAZ [15, 36, 37]. However, investigations about the influence of the weld penetration profile on the HAC susceptibility of a high-strength steel due to different welding process characteristics do not exist so far.

For that purpose, the aim of the present study is to determine the HAC susceptibility in the HAZ of micro-alloyed high-strength steel S960QL with a similar micro-alloyed filler material. Comparative studies are carried out using the Conv.

Fig. 1 Comparison of layer build-up in 20-mm-thick multi-layer welds on steel S960QL: (a) Conv. A at 60°-V-groove (8 weld beads) and (b) Mod. SA at 30°-V-groove (3 weld beads) [19].
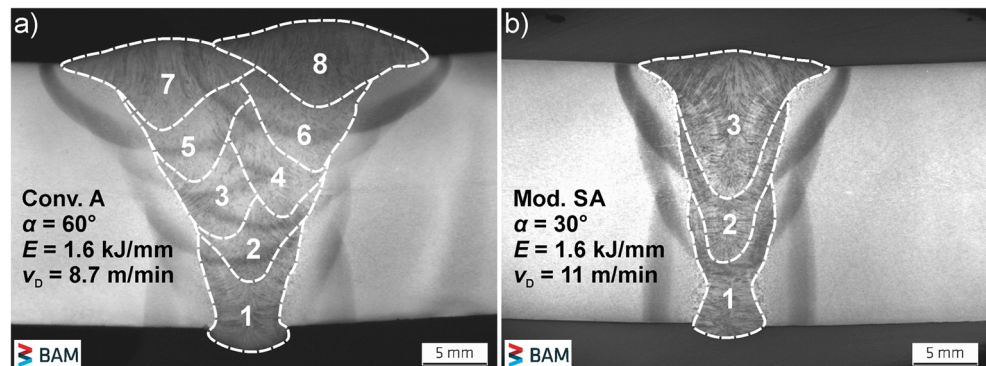
A and the Mod. SA. The focus is on the deeper weld penetration profile when using the Mod. SA with increased deposition rate. In addition, heat input is kept constant. Implant tests are accompanied by ISO 3690 [38] weldments to determine the diffusible hydrogen concentration H_D in arc weld metal. Further analysis by light optical microscopy, hardness testing, and scanning electron microscopy is used to discuss microstructure and fracture behavior. Based on the results, the determination of the maximum stress for avoiding HAC "critical implant stress" σ_{crit} is used to calculate the embrittlement index EI. It must be mentioned that the results from these implant tests cannot be transferred to real welded components of high-strength steels regarding HAC in welding processing. This requires the consideration of all three main factors influencing HAC.

2 Materials and methods

2.1 Materials

For the experimental investigations, the high-strength structural steel S960QL according to EN 10025-6 [39] with a sheet thickness of 20 mm was used. This steel can be highly susceptible to HAC [14, 15]. The filler material used was the solid wire G 89 6 M Mn4Ni2CrMo according to ISO 16834-A [40] with a wire diameter of 1.2 mm. The chemical composition and mechanical properties of the test materials are listed in Table 1 and Table 2.

2.2 Implant test

The HAC susceptibility in the HAZ of the S960QL when using Conv. A and Mod. SA was tested by the implant test according to ISO 17642-3 [41]. This cold cracking test is subjected to an external stress, in which the external load can be set in a defined manner. Figure 2 shows the geometry of the specimens and the test configuration. To carry out the implant tests, implant specimens with a test diameter of 6 mm and a circumferential spiral notch according to the standard were machined from the 20-mm-thick plate (see Fig. 2a). The implant specimen was inserted into one of three holes of an unalloyed structural steel plate (200 mm × 300 mm × 20 mm) so that the face is flush with the surface of the plate (see Fig. 2b and Fig. 2c).

Before welding, the surfaces were cleaned with acetone. To ensure a crack-critical microstructure with high hardness in the HAZ, all welds were carried out without preheating. Bead-on-plate welds were conducted using the welding processes and parameters from Table 3, which were adapted to the investigations in [19, 20]. The higher wire feed speed (deposition rate) when using the Mod. SA required a higher welding speed to keep the heat input constant compared with Conv. A (see Table 3). The used shielding gas was ISO 14175-M21-ArC-18 with a gas flow of 18 l/min. During welding, type-K-thermocouples (diameter 0.8 mm) were plunged into the molten pool to record the temperatures vs. time $T(t)$ during cooling. Based on these temperature curves, the cooling times were determined afterwards. The $t_{8/5}$-cooling time (time difference between 800 and 500 °C) was used to discuss the microstructure in weld metal and HAZ. The $t_{3/1}$-cooling time (time difference between 300 and 100 °C) was used to describe the stability of the arc process and the heat transfer in the sample. Immediately after welding, the implant specimens were preloaded with approximately 50 MPa to avoid internal looseness in the loading device. During cooling to temperatures between 150 and 100 °C, the samples were then subjected to a defined static tensile load within 20 to 60 s according to the standard [41]. The time to failure (TTF) of the implant specimen was registered as a function of the applied stress. The maximum load duration was 48 h to take account of time-delayed HAC. The standard [41] recommends a minimum of 16 h. Figure 3 shows an example of the recording of the force/stress and temperature over time. The aim of the implant tests was to enable a qualitative estimation (fracture or no fracture) and the quantitative determination of the maximum stress that can be achieved to avoid cracking in the HAZ.

It is important to note that the geometry of the implant specimen of the ISO 17642-3 [41] is different from that described in the AWS B4.0 standard [42]. In accordance with the AWS standard, the critical stress value for complete fracture, which is the "lower critical stress" LCS, of the specimen is used for evaluation of the HAC susceptibility in the HAZ [33,

Table 1 Chemical composition of test materials (Fe—balance)

Element in %	C	Si	Mn	Mo	Cr	Cu	Ni	V	Ti	Nb	CET*	CE$_{IIW}$**
Base material (a) S960QL, h = 20 mm	0.17	0.32	0.95	0.33	0.58	0.020	0.92	0.056	0.002	0.017	0.35	0.58
Filler material (b) G 89 6 M Mn4Ni2CrMo	0.10	0.81	1.77	0.57	0.38	0.013	2.22	0.003	0.047	0.003	0.41	0.73

(a) Measured by optical emission spectroscopy, (b) according to manufacturer's certificate

*CET according to EN 1011-2/C.3

**CE$_{IIW}$ according to EN 1011-2/C.2

Table 2 Mechanical properties of test materials

Property	Yield strength $R_{p0.2}$ in MPa	Tensile strength R_m in MPa	Elongation A_5 in %	Impact toughness A_v in J
Base material (a)				
S960QL, $h = 20$ mm	1065	1116	10	54 (-40 °C)
Filler material (b)				
G 89 6 M Mn4Ni2CrMo	938	980	15	62 (-60 °C)

(a) Mechanical testing, (b) according to manufacturer's certificate

34, 36, 37]. In the present study, the incipient crack is used as criterion to determine the critical stress level according to [41]. For this reason, "critical implant stress" σ_{crit} for avoiding cracks in the HAZ is defined in addition to LCS. As already shown in previous investigation [15], σ_{crit} was used to calculate the embrittlement index EI.

2.3 Hydrogen measurement in arc weld metal

The implant tests were accompanied by welding experiments to determine the diffusible hydrogen concentration in the arc weld metal. For that purpose, test welds were produced according to ISO 3690 standard [38] with both welding processes (Conv. A and Mod. SA) using the welding parameters listed in Table 3. For the test welds, the ISO 3690 sample type "B" was used with dimensions 15 mm × 30 mm × 10 mm of test specimen. The specimens were clamped in a water-cooled welding fixture (see Fig. 4). Subsequently after welding, the samples were removed from the fixture and quenched in ice

water and stored in liquid nitrogen according to the standard [38]. After the specimens were completely frozen, they were removed from liquid nitrogen and the starting and runoff weld tabs were struck off with a hammer and the test specimens were frozen again. For hydrogen analysis, the test specimens were first removed from the liquid nitrogen and heated up for 60 s in ethanol to room temperature. Subsequently, the specimens were heated up to 400 °C in an infrared furnace. The desorbing hydrogen was collected and analyzed by carrier gas hot extraction (CGHE). In contrast to the methods suggested in ISO 3690 [38], a mass spectrometer (MS) was used to detect the diffusible hydrogen due to its higher resolution and, hence, more reliable results in terms of low hydrogen concentrations. More details about carrier gas hot extraction and MS principle can be found in [20, 43, 44]. Since the amount of hydrogen is related to the volume of the arc weld metal, its mass is required. The mass corresponds to the difference weight of the specimen before and after welding. With the integrated ion current of MS vs. time, a previous

Fig. 2 Schematic illustration of implant test: (a) geometry of the implant specimen, (b) geometry of specimen plate, and (c) test configuration [15]
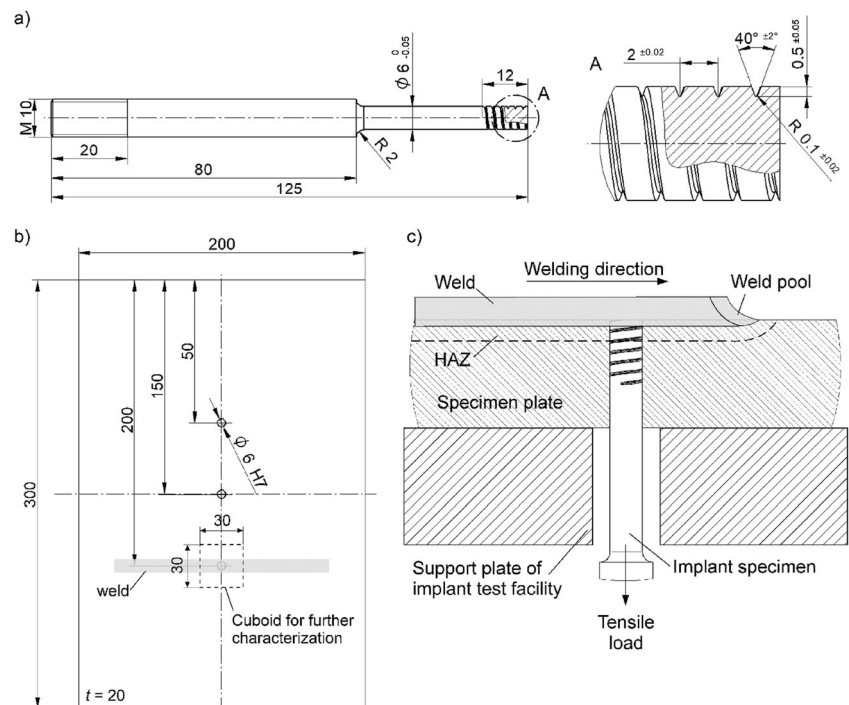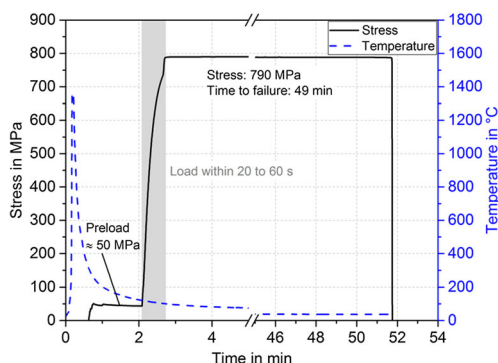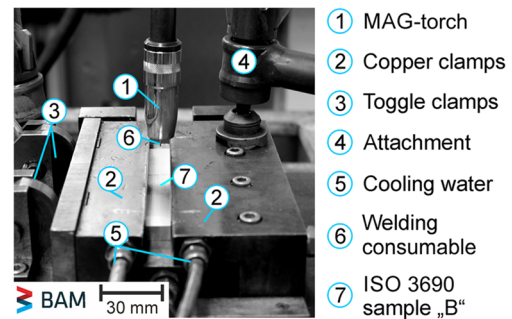
Table 3 Welding parameters for the implant tests

Welding process	Conv. A	Mod. SA
Wire feed speed v_D in m/min	8.7	11
Arc voltage U in V	26.5 ± 0.1	29 ± 0.1
Welding current I in A	275 ± 15	328 ± 10
Welding speed v_S in cm/min	27	35
CTWD in mm	17	18
Heat input E in kJ/mm	1.6	1.6

determined calibration factor, and the mass, the diffusible hydrogen concentration H_D was calculated in µg/g, which corresponds to 1.11 ml/100 g of arc weld metal.

2.4 Further methods for characterization

Cuboids with a size of 30 mm × 30 mm × sheet thickness were cut out of all welded specimens for further investigations (see Fig. 2b). In the case of non-ruptured specimens, three longitudinal sections in weld bead direction (each 1.5 mm apart) according to the standard [41] were machined via electric discharge machining (EDM) (see Fig. 5). They had been used for the metallographic examination for incipient cracks at magnification factor of ×400 and ×600. To determine the fracture position of the implant specimens, macro-sections were taken transversely to the welding direction (see Fig. 5). Furthermore, ISO 3690 specimens were used to study the weld penetration profile of both arc processes. All metallographic specimens were embedded, ground, polished and etched with 2% Nital (HNO_3), and examined under light optical microscopy. The investigations were accompanied by hardness tests in weld metal, HAZ, and base material using a load of 9.807 N (HV 1) and 98.07 N (HV 10). The analysis of the fracture surfaces of the ruptured implant specimens was carried out with the scanning electron microscope (SEM) VEGA3 TESCAN with an accelerated voltage of 20 kV.


Fig. 4 Welding fixture for ISO 3690 welding with clamped sample in accordance with [44]

① MAG-torch
② Copper clamps
③ Toggle clamps
④ Attachment
⑤ Cooling water
⑥ Welding consumable
⑦ ISO 3690 sample „B"

3 Results and discussion

3.1 Cooling times and hydrogen concentration in arc weld metal

Figure 6 summarizes the cooling times of the implant tests and the diffusible hydrogen concentrations H_D determined in the arc weld metal. As already shown in the results of joint welds with V-groove [19–21], the use of the Mod. SA results in slightly shorter $t_{8/5}$-cooling times than when using the Conv. A. Consequently, the $t_{3/1}$-cooling times differ. However, the low scattering of the cooling times indicates stable arc processes. When welding with Mod. SA with higher deposition rate, 1.6 ml/100 g of diffusible hydrogen is present in the arc weld metal. This value is approx. 23% higher than the hydrogen concentration of 1.3 ml/100 g of arc weld metal when using Conv. A.

As moisture in the shielding gas is strictly limited [45], it is to be assumed that the main source for diffusible hydrogen is the filler material. The used solid wire contains 2.2 ml/100 g of total hydrogen concentration in delivery condition [20]. During welding, this concentration can be introduced into the weld metal, whereby the wire feed speed has the largest effect [20]. The higher wire feed speed in case of Mod. SA results in an increase in welding current of about 50 A (cf. Table 3). Due to this, more hydrogen can be dissociated in the arc and absorbed by the weld metal [20, 46, 47]. In addition, an increased amount of hydrogen is available with increased

Fig. 3 Exemplary recording of stress and temperature vs. time
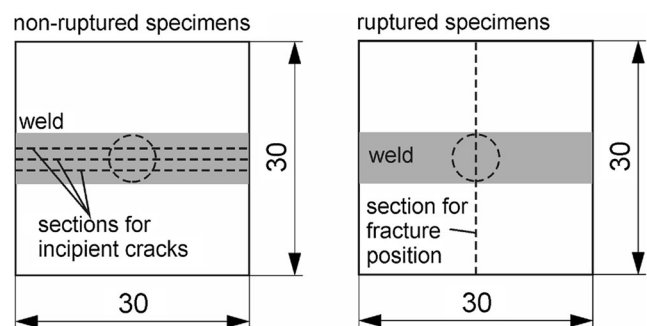
Fig. 5 Samples and extraction positions for further metallographic characterization
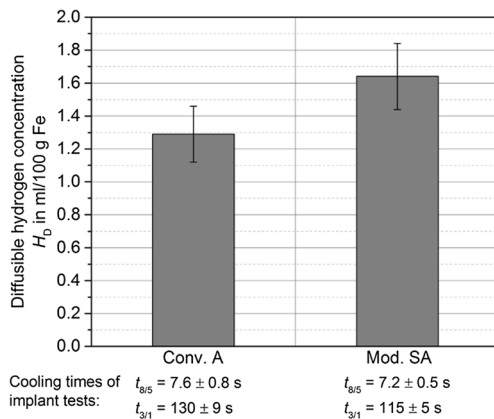
Fig. 6 Diffusible hydrogen concentration H_D in arc weld metal and average determined cooling times of the implant tests

wire feed speed. Investigations using a metal-cored wire showed the same tendency [48]. If more hydrogen is added to the shielding gas, H_D can reach 6 ml/100 g [49]. In this case, the difference between the two arc processes disappears, since the shielding gas is then the main source of hydrogen. Furthermore, H_D of 1.6 ml/100 g can also be present in case of Conv. A if a different solid wire is used [15]. Nevertheless, for the present test materials, the determined hydrogen concentrations between 1.3 and 1.6 ml/100 g are critical regarding HAC [14, 15].

3.2 Results of implant tests with two arc processes

Figure 7 shows the results of the implant tests as a plot of the implant stress over the TTF for both Conv. A (Fig. 7a) and Mod. SA (Fig. 7b). For both test series, with reduced implant stress, the TTF increases significantly. When the Conv. A is used, samples fail until 555 MPa applied stress. In case of Mod. SA, the samples fail until a stress of approx. 504 MPa. The difference of 51 MPa of the so-called lower critical stress (LCS) is discussed later in Section 3.3. Implant tests on the same base material using a metal-cored wire showed the same behavior [48]. Implant samples loaded below LCS initially showed no failure after 48 h (see Fig. 7).
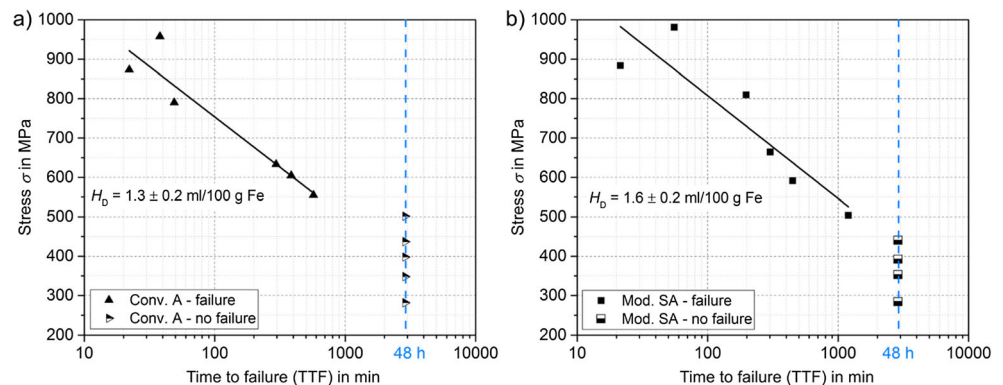
With the ratio of LCS to the nominal yield strength of the base material, the normalized critical stress ratio (NCSR) can be calculated [15, 31]. The NCSR in case of Conv. A and Mod. SA is 0.58 and 0.53, respectively. These results show similar behavior to investigations in [15, 36, 37] with materials of 690 to 1100 MPa yield strength. But in [36, 37], diffusible hydrogen concentrations 4 to 5 times higher than in the present study (6.5 ml/100 g of arc weld metal) existed. Thus, it is reasonable to assume a very high susceptibility to HAC for the present high-strength steel, regardless of the used welding arc process.

3.3 Weld microstructure and cracks in implant specimens

Figure 8 shows cross-sections of the fracture position of welded implant specimens for both Conv. A (Fig. 8a) and Mod. SA (Fig. 8b). In both parts, the geometry of the original implant specimens is indicated before the loading was applied. It can be seen that the fracture occurs at the notch root of the implant specimen in the HAZ through the weld metal in both cases. This fracture location was observed for all failed specimens.

The hardness distribution of weld metal, HAZ, and base material of samples welded with Conv. A and Mod. SA with a longitudinal section and the corresponding hardness indentations are illustrated in Fig. 9. Due to the slight undermatching, the weld metal shows lower hardness from 275 to 300 HV 1 in both cases than the base material, which has hardness from 350 to 375 HV 1. Due to the high carbon content of 0.17% of the base material, the coarse-grained HAZ (CGHAZ) shows a pronounced hardening. When using the Mod. SA, the maximum hardness in CGHAZ is 453 HV 1 and for Conv. A, it is 439 HV 1. The hardness measurement in HV 10 shows qualitatively similar hardness distributions. For Mod. SA, the maximum hardness is 423 HV 10 and for Conv. A, it is 411 HV 10. The small differences between the maximum hardness values in both cases can be explained on the one hand by the scattering of the two welding tests and the measurement inaccuracy in the hardness test (8% for HV 1 and 4%

Fig. 7 Implant test curves of S960QL: (a) welded with Conv. A and (b) welded with Mod. SA

Fig. 8 Cross-sections to the welding direction to determine the fracture position of the implant specimens: (a) Conv. A and (b) Mod. SA
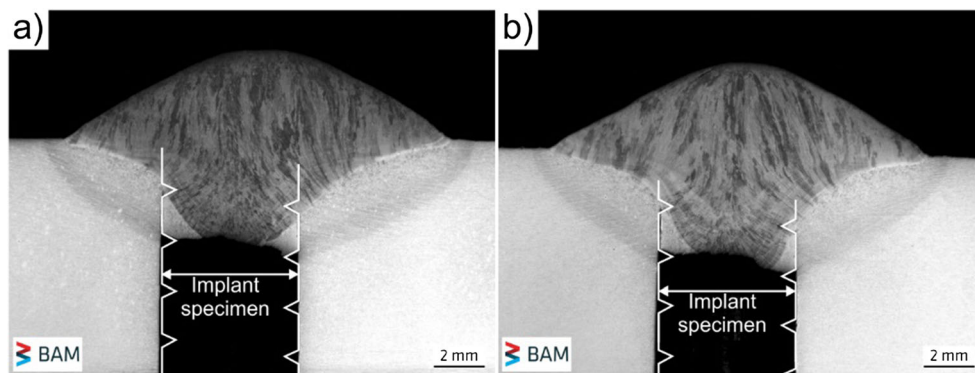
for HV 10) according to ISO 6507-2. On the other hand, the higher hardness values in case of the Mod. SA may be due to the slightly faster cooling. Especially at the interface from the HAZ to the weld metal, welding with Mod. SA results in a higher hardness than with Conv. A. This behavior was also reported in [48] when using a metal-cored wire. This difference in hardness can explain the lower LCS when using Mod. SA.

The weld metal consists of a mixture of bainitic and martensitic phase at the determined $t_{8/5}$-cooling times of 7 to 8 s [50]. The distinction between martensite and bainite in the CGHAZ of the used material is very difficult. Therefore, the microstructure was additionally characterized by calculating the maximum hardness HV_M for a purely martensitic microstructure according to Dueren [51]. For the used S960QL, HV_M is 441 HV 10 in the CGHAZ. As the maximum measured hardness is 411 HV 10 and 423 HV 10 in case of Conv. A and Mod. SA, respectively, there are small amounts of bainite in the CGHAZ (see Fig. 10). The shown microstructure is similar to that of the CGHAZ of a S960QL with a comparable chemical composition in previous investigation [15].

In numerical investigations on implant tests [52] in case of S690QL and S1100QL, the highest local stresses and strains occur in the area at the notch root of the implant specimen. Also, in the case of notched tensile specimens with a martensitic microstructure, the influence of hydrogen becomes less important at very high applied stresses [53]. With lower applied stresses, the diffusible hydrogen that is introduced into the weld metal diffuses into these highly strained regions [52]. Thus, there is a critical combination of the three influencing factors on HAC in the CGHAZ at the notch root of the implant specimen: a highly HAC-susceptible microstructure with high hardness, highly mechanically strained area, and locally increased hydrogen concentration. As a result, micro-cracks arise at this point, which grow into the weld metal at
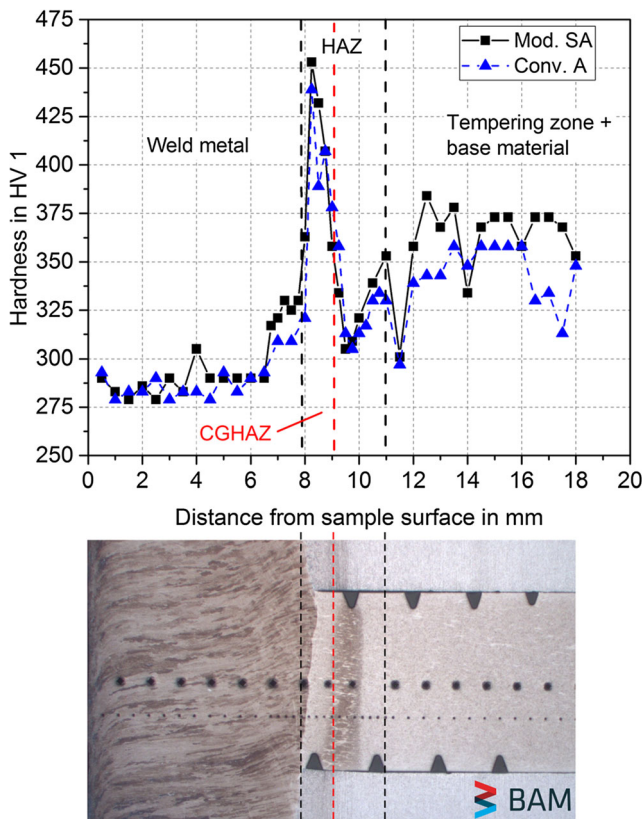

Fig. 9 Vickers hardness measurements along the axis of the implant sample taken on a macro-section transversely to the welding direction for Conv. A and Mod. SA
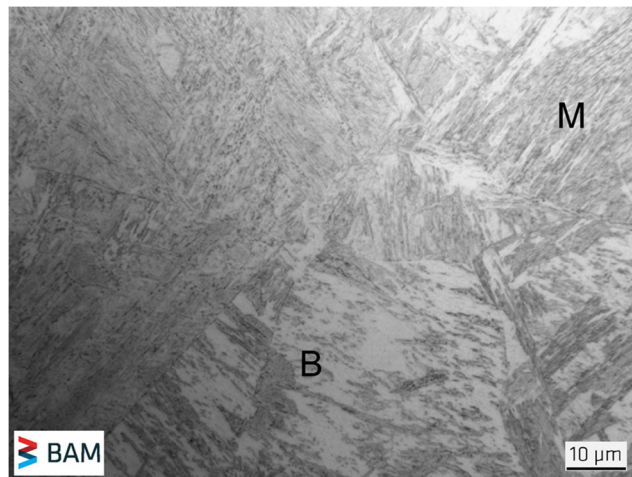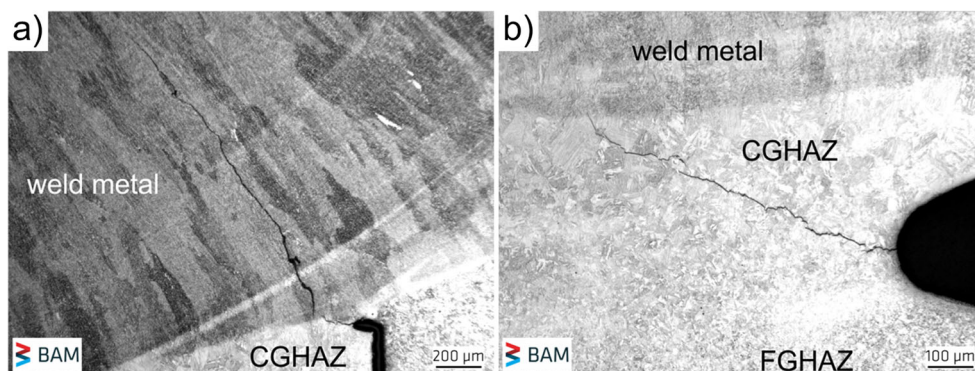

Fig. 10 Microstructure in the CGHAZ at $t_{8/5} = 7$ s

mechanical stresses above 400 MPa (Fig. 11a) and arrest at the fusion line at lower stresses of less than 400 MPa (Fig. 11b). The maximum stress without cracking σ_{crit} is 280 MPa for both types of arc processes.

Using ISO 18265 standard [54], the corresponding ultimate tensile strength can be calculated from the maximum hardness values in the CGHAZ. In the case of Conv. A, the hardness of 411 HV 10 corresponds to a tensile strength of 1323 MPa and in the case of Mod. SA, the hardness of 423 HV 10 corresponds to a tensile strength of 1360 MPa. The ratio of the critical implant stress σ_{crit} to the tensile strength of CGHAZ

is used to calculate the embrittlement index EI. The EI was 0.21 for both cases as the calculated tensile strength was nearly identical. So far, the results indicated that the tested material S960QL has the same HAC susceptibility in the CGHAZ for both types of arc processes. As mentioned in Section 2.1, in most investigations, the implant geometry of AWS standard [42] is used. Here, the LCS is used instead of σ_{crit} to calculate the EI. Yue [37] showed for a comparable 690 MPa grade steel a similar EI of 0.24 at significantly increased hydrogen concentration of 10.5 ml/100 g of arc weld metal. This contrasts with our study, as the examined S960QL already shows
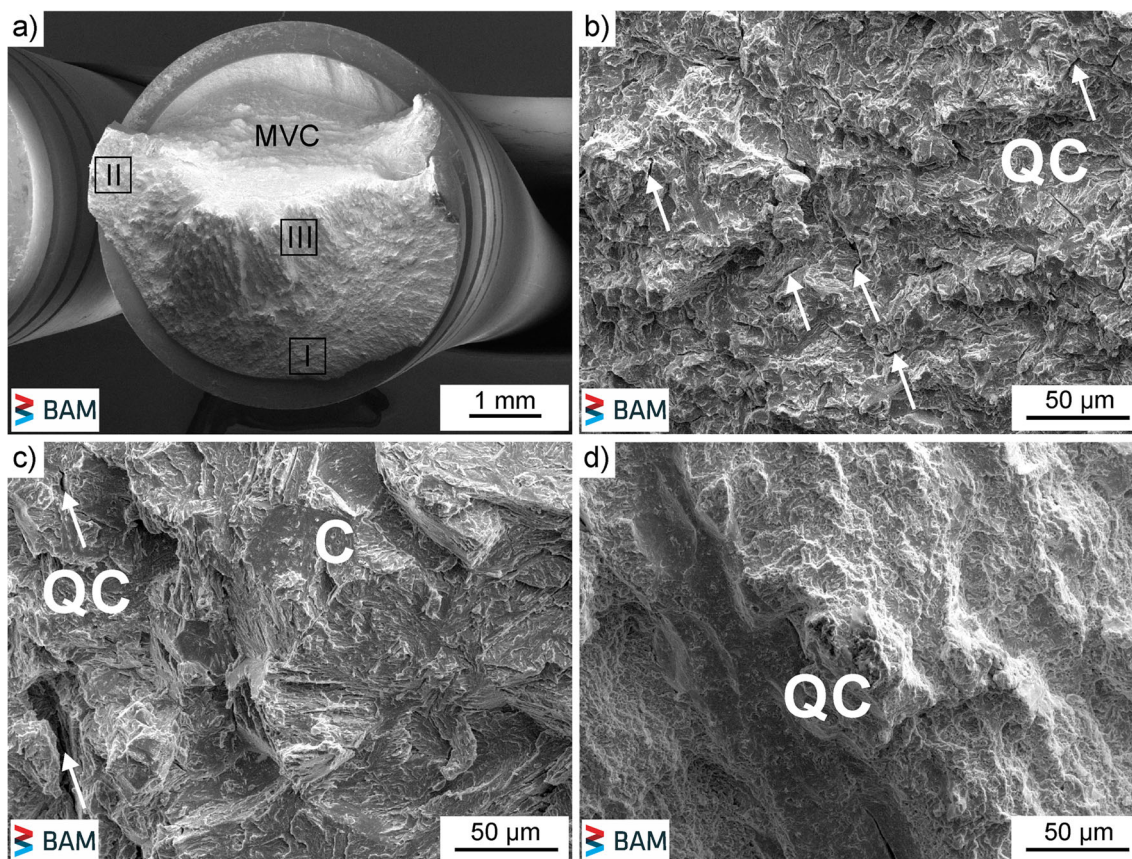

Fig. 12 Fracture topography of implant sample welded with Conv. A—σ = 605 MPa: (a) fracture overview, (b) region I—QC, (c) region II—QC and C, and (d) region III—QC; white arrows indicate secondary cracks
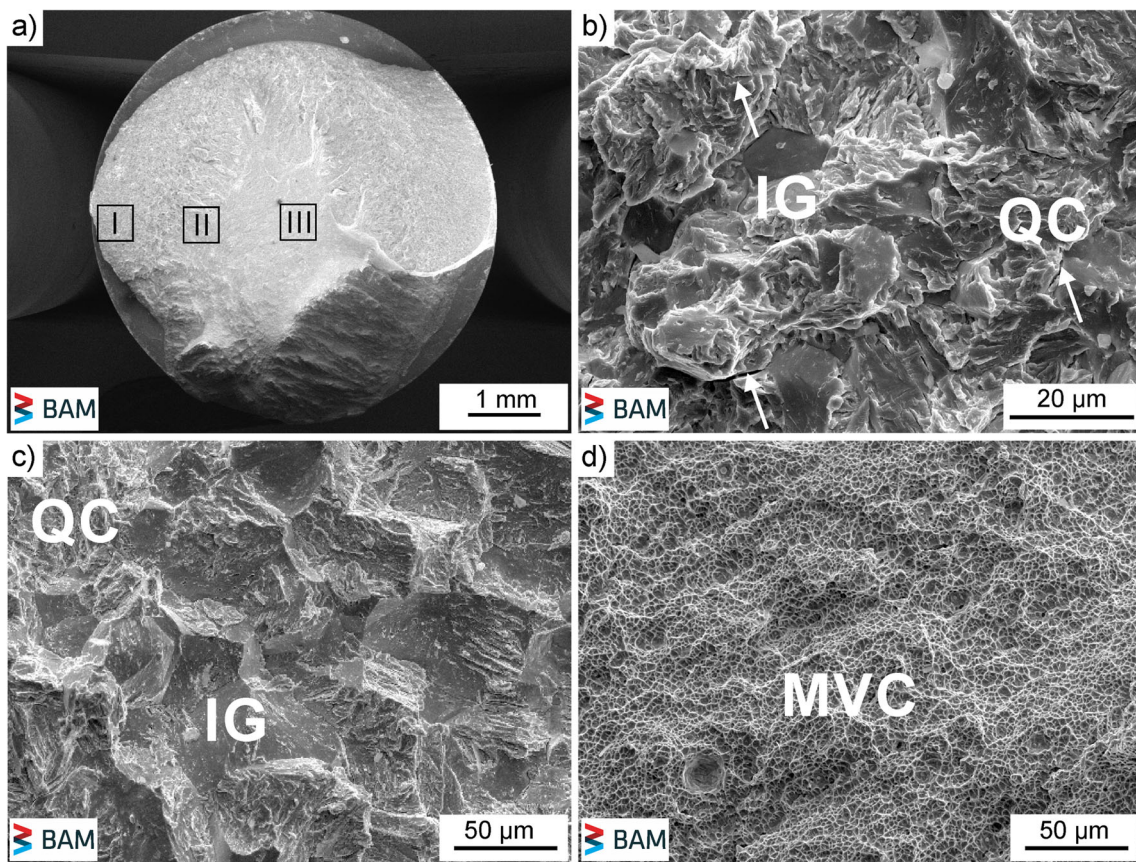
Fig. 13 Fracture topography of implant sample welded with Mod. SA—σ = 591 MPa: (a) fracture overview, (b) region I—QC and IG, (c) region II—QC and IG, and (d) region III—MVC; white arrows indicate secondary cracks

an EI of 0.21 at hydrogen concentrations of 1.3 to 1.6 ml/ 100 g of arc weld metal, which is approximately 6 to 8 times lower. In addition to the NCSR, this is a further indicator of the high HAC-susceptibility in the HAZ of welded S960QL.

3.4 Fracture behavior

The fracture behavior when welding with Conv. A and Mod. SA has been investigated by SEM (see Fig. 12 and Fig. 13). In that connection, the fracture surface could be separated into three regions of interest where significant differences in the

fracture topography occurred. They are denoted in the following: region I (area of crack initiation), region II (transition zone), and region III (bulk fracture surface). The fracture topography of the ruptured implant specimens with Conv. A was quasi-cleavage (QC) in region I (see Fig. 12b). Region II showed also a QC-like fracture topography with small undeformed cleavage (C) fracture surfaces (see Fig. 12c). In the bulk material, the fracture topography was ductile with microvoid coalescence (MVC) and QC in region III (see Fig. 12d). Regions I and II also showed secondary cracks, which are typical for the influence of hydrogen in high-strength

Fig. 14 (a) Regression functions of the implant stress vs. TTF (from Fig. 7) without measurement points; (b) corresponding TTF difference vs. applied implant stress
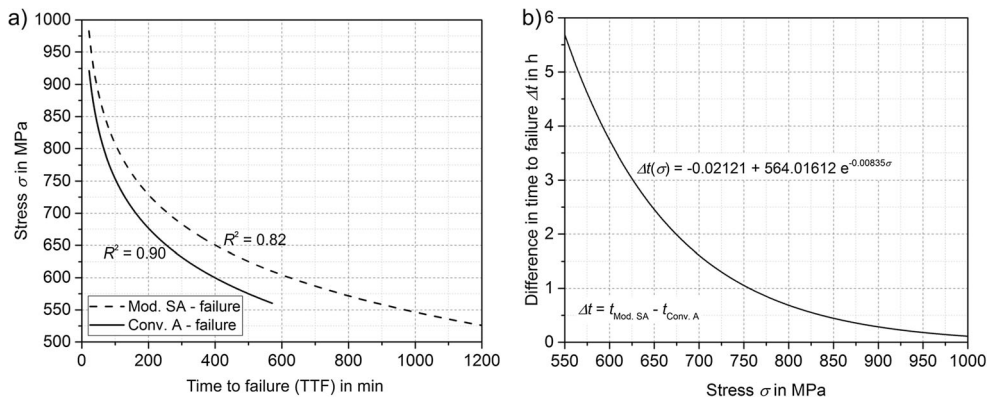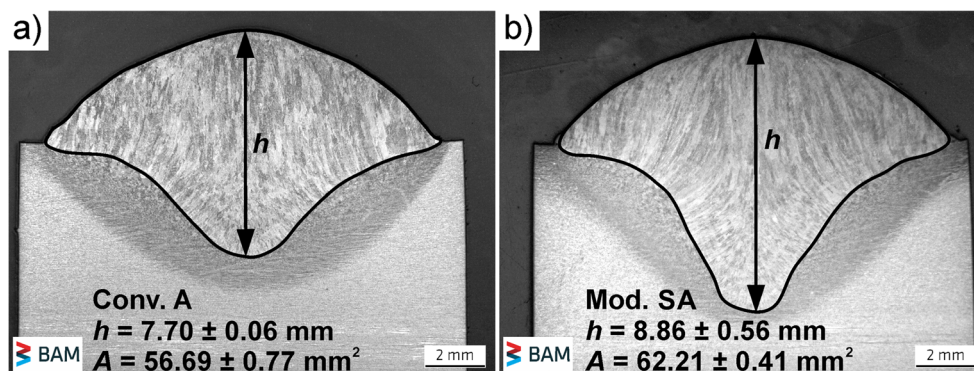
Fig. 15 Cross-sections of bead-on-plate welds and corresponding weld penetration depth and average area of weld metal: (a) Conv. A with $v_D = 8.7$ m/min and (b) Mod. SA with $v_D = 11$ m/min

structural steels [55]. The distinction between QC and C fracture surfaces is based on the fact that areas without any deformation are present. This is also shown in welded microstructures of a low-alloyed heat-resistant steel [53].

When using Mod. SA, the fracture topography changed to primarily QC fracture with shares of intergranular (IG) fracture and secondary crack appearance in regions I and II (see Fig. 13b and Fig. 13c). The topography in region III showed MVC (see Fig. 13d). The higher hydrogen concentration in case of Mod. SA (Fig. 6) causes more IG fracture surfaces. Added to this are the slightly lower cooling times and the higher hardness in the CGHAZ, according to which the microstructure tends more towards IG cracking behavior.

The occurrence of the mainly IG, QC, and MVC fracture topography on the implant specimen surface can be explained by Beachem's model [55]. The author investigated a wedge-loaded specimen in hydrogen environment. Therefore, the fracture behavior depends on the combination of hydrogen concentration and stress intensity factor at the crack tip. Gedeon [56] substantiated Beachem's work on implant tests and extended the model. When the implant specimen is mechanically loaded after welding, the hydrogen concentration in the highly stressed region is not high enough to initiate cracking. During an incubation period, hydrogen diffuses into this highly stressed and strained region and reaches the critical concentration at some time. In the CGHAZ, a crack is then initiated and appears as intergranular topography for a short

distance. When the crack propagates, the stress intensity factor increases and the hydrogen concentration at crack tip decreases. A QC fracture topography is then promoted. With further crack growth, the stress intensity factor increases further with decreasing level of hydrogen concentration, which leads to MVC fracture mode until ultimate failure takes place.

If comparing Fig. 12 and Fig. 13, intergranular areas are obvious when using Mod. SA. In this case, there is a higher hydrogen concentration at the crack tip which has the effect of decreasing the stress intensity factor. This leads to IG fracture topography [55, 56]. However, the hydrogen concentration is too low for IG fracture topography when using the Conv. A.

3.5 Influence of weld penetration depth

The results show the comparative behavior between Conv. A and Mod. SA (whereas Mod. SA is characterized by increased deposition rate). The increased deposition rate leads to the advantages already mentioned above, such as shorter welding times and lower production costs [17, 18]. But a difference of about 50 MPa for LCS between both welding processes and more pronounced IG fracture topography in case of Mod. SA were observed. However, a closer look at the results in Fig. 7 revealed a clear difference regarding the TTF. Figure 14a illustrates the two regression functions of the test series welded with Conv. A and Mod. SA. The deviating TTF for a constant applied stress can be clearly seen. With these two graphs, the

Table 4 Implant test results

Welding process	CGHAZ max hardness in HV 10	CGHAZ tensile strength[a] in MPa	Lower critical stress (LCS) in MPa	Critical implant stress σ_{crit} in MPa	Normalized critical stress ratio (NCSR)[b]	Embrittlement index (EI)[c]	Time to failure at LCS in min
Conv. A	411	1323	555	280	0.58	0.21	571
Mod. SA	423	1360	504	280	0.53	0.21	1199

[a] Calculated from maximum hardness in CGHAZ according to ISO 18265

[b] LCS normalized to nominal base material yield strength (960 MPa)

[c] Critical implant stress normalized to calculated CGHAZ tensile strength

difference for a constant applied stress was calculated. The calculated difference of both TTF functions for a constant implant stress value is plotted in Fig. 14b.

While the specimens failed simultaneously at 1000 MPa, the time difference increases exponentially to almost 6 h at a stress of 550 MPa. The samples welded with Mod. SA therefore fail with a time delay. This time difference can be related to the different weld penetration profiles of both arc variants. In the cross-sections in Fig. 15, the deeper weld penetration is visible in the case of the sample welded with Mod. SA. Due to the higher deposition rate at a very short arc length, the deeper penetration causes longer diffusion paths for the hydrogen into the crack-critical areas under the assumption that the hydrogen is distributed homogeneously in the weld metal after welding [19, 57]. A critical hydrogen concentration is therefore achieved only at a later stage at deeper penetration. Studies using a metal-cored wire with higher level of hydrogen concentration showed for the same welding parameters and base material that implant specimens fail within 200 min until applied stresses of 600 MPa, regardless of the used welding process [48]. At lower stresses, also a shift of TTF to longer times existed in the case of Mod. SA. Although this time difference was not so significant, there was a strong HAC susceptibility due to $H_D \geq 2.8$ ml/100 g of arc weld metal, regardless of the used arc or the weld penetration profile.

Table 4 summarizes the implant test results. The Mod. SA welded test series shows a higher hardness in the CGHAZ, which is due to the slightly shorter cooling times or measurement inaccuracy in hardness testing. Accordingly, there is a slightly higher tensile strength in this area. The critical implant stress, however, is 280 MPa for both cases. The EI in both test series corresponds to about 0.21. The TTF at LCS shows a significant difference between the conducted test series. The specimen welded by Mod. SA has a TTF (1199 min)—twice as long as the specimen welded by Conv. A (571 min).

4 Conclusions

In the present study, the HAC susceptibility in the HAZ of the micro-alloyed high-strength structural steel S960QL with a similar micro-alloyed welding filler material was analyzed using the externally loaded implant test. The use of two different arc variants (Conv. A and Mod. SA) with the same heat input and different deposition rate allowed investigations of the influence of the weld penetration depth on the HAC behavior. Under the used welding parameters, the following conclusions can be drawn:

- As has already been shown in [19–21], the use of Mod. SA with an increased deposition rate can lead to higher hydrogen concentrations than in welds welded by Conv. A. However, the hydrogen concentrations present in both cases are critical for the used materials [14, 15].

- All incipient cracks in the implant specimens occurred in the notch root of the spiral notch in the CGHAZ under maximum stress and high local hydrogen concentration. The crack propagation took place from the initial crack into the weld metal.

- Regardless of the arc process, a critical implant stress of 280 MPa for crack-free operation was determined. This corresponds to about 30% of the nominal yield strength of the base material.

- The "embrittlement index" EI describes the ratio of critical implant stress to the tensile strength of CGHAZ. The EI in both cases is 0.21. This clearly shows the high susceptibility of the used material to HAC at hydrogen concentrations $H_D \geq 1$ ml/100 g.

- The deeper penetration profile when using the Mod. SA with increased wire feed speed can cause longer diffusion paths for the hydrogen into the crack-critical areas. In addition, a changed direction of solidification of weld metal is possible with deeper penetration which can influence the hydrogen diffusion in terms of preferred direction and therefore time [58]. Consequently, TTF of the implant specimens increases significantly. In addition, the higher hydrogen concentrations can cause intergranular areas on the fracture surfaces.

For a general assessment of the risk against HAC of a real welded component made of high-strength structural steels, all three influencing factors must be considered. By adjusting the welding parameters, for example, the diffusible hydrogen concentration in arc weld metal can be lowered [20] and welding loads can be reduced using Mod. SA at smaller weld seam opening angles [59].

References

1. Ahlblom B, Hansson P, Narström T (2007) Martensitic structural steels for increased strength and wear resistance. Mater Sci Forum 539-543:4515–4520. https://doi.org/10.4028/www.scientific.net/MSF.539-543.4515

2. Hulka K, Kern A, Schriever U (2005) Application of niobium in quenched and tempered high-strength steels. Mater Sci Forum 500-501:519–526. https://doi.org/10.4028/www.scientific.net/MSF.500-501.519

3. Gliner RE (2011) Welding of advanced high-strength sheet steels. Weld Int 25(5):389–396. https://doi.org/10.1080/09507116.2011.554234

4. EN 1011–2 (2001) Welding – recommendations for welding of metallic materials – part 2: arc welding of ferritic steels

5. CEN ISO/TR 17844 (2004) Welding – comparison of standardised methodes for the avoidance of cold cracks

6. Zeman M (2009) Assessment of weldability of WELDOX 1100 high-strength quenched and tempered steel. Weld Int 23(2):73–82. https://doi.org/10.1080/09507110802349122

7. ANSI/AWS D1.1/D1.1M (2015) Structural welding code – steel. American Welding Society

8. Villalobos JC, Del-Pozo A, Campillo B, Mayen J, Serna S (2018) Microalloyed steels through history until 2018: review of chemical composition, processing and hydrogen service. Metals 8(5):351. https://doi.org/10.3390/met8050351

9. Zhang L, Kannengiesser T (2016) HAZ softening in Nb-, Ti- and Ti + V-bearing quenched and tempered steel welds. Weld World 60(2):177–184. https://doi.org/10.1007/s40194-016-0299-7

10. Grabke HJ, Riecke E (2000) Absorption and diffusion of hydrogen in steels. Mater Technol 34(6):331–342

11. Thomas A, Szpunar JA (2020) Hydrogen diffusion and trapping in X70 pipeline steel. Int J Hydrog Energy 45:2390–2404. https://doi.org/10.1016/j.ijhydene.2019.11.096

12. Park C, Kang N, Liu S (2017) Effect of grain size on the resistance to hydrogen embrittlement of API 2W grade 60 steels using in situ slow-strain-rate testing. Corros Sci 128:33–41. https://doi.org/10.1016/j.corsci.2017.08.032

13. Zhang S, Huang Y, Bintang S, Qingliang L, Hongzhou L, Jian B, Mohrbacher H, Zhang W, Guo A, Zhang Y (2015) Effect of Nb on hydrogen-induced delayed fracture in high strength hot stamping steels. Mater Sci Eng A 626:136–143. https://doi.org/10.1016/j.msea.2014.12.051

14. Zimmer P, Seeger DM, Boellinghaus T (2005) Hydrogen permeation and related material properties of high strength structural steels. In: High strength steels for hydropower plants. Verlag der Techn. Univ. Graz, Graz, pp 1-18, paper 17

15. Schaupp T, Ernst W, Spindler H, Kannengiesser T (2020) Hydrogen-assisted cracking of GMA welded 960 MPa grade high-strength steels. Int J Hydrog Energy 45(38):20080–20093. https://doi.org/10.1016/j.ijhydene.2020.05.077

16. Iordachescu D, Quintino L (2008) Steps toward a new classification of metal transfer in gas metal arc welding. J Manuf Process 202(1–3):391–397. https://doi.org/10.1016/j.jmatprotec.2007.08.081

17. Cramer H, Baum L, Pommer S (2011) Überblick zu modernen Lichtbogenprozessen und deren Werkstoffübergängen beim MSG-Schweißen (Overview of modern arc processes and their material transitions in GMA welding). In: DVS-Berichte 275. DVS Media GmbH, Düsseldorf, pp 232–237 (in German)

18. Norrish J (2017) Recent gas metal arc welding (GMAW) process developments: the implications related to international fabrication standards. Weld World 61(4):755–767. https://doi.org/10.1007/s40194-017-0463-8

19. Schaupp T, Rhode M, Yahyaoui H, Kannengiesser T (2019) Influence of heat control on hydrogen distribution in high-strength multi-layer welds with narrow groove. Weld World 63(3):607–616. https://doi.org/10.1007/s40194-018-00682-0

20. Schaupp T, Rhode M, Kannengiesser T (2018) Influence of welding parameters on diffusible hydrogen content in high-strength steel welds using modified spray arc process. Weld World 62(1):9–18. https://doi.org/10.1007/s40194-017-0535-9

21. Schröpfer D, Schaupp T, Kannengießer T (2019) Kaltrissvermeidung in Schweißverbindungen aus hochfesten Feinkornbaustählen bei engen Nahtspalten und fokussiertem Lichtbogen. In: Fortschrittsberichte der Materialforschung und Werkstofftechnik. Shaker Verlag, Aachen, pp 377–389 (in German)

22. Fydrych D, Świerczyńska A, Tomków J (2014) Diffusible hydrogen control in flux cored arc welding process. Key Eng Mater 597:171–178. https://doi.org/10.4028/www.scientific.net/KEM.597.171

23. Mente T, Boellinghaus T, Schmitz-Niederau M (2012) Heat treatment effects on the reduction of hydrogen in multi-layer high-strength weld joints. Weld World 56(7–8):26–36. https://doi.org/10.1007/BF03321362

24. Wongpanya P (2008) Effects of heat treatment procedures on the cold cracking behaviour of high strength steel welds. Dissertation, Helmut Schmidt University Hamburg, BAM-Dissertationsreihe, Band 36. ISBN: 978-3-9812072-7-9

25. Kannengiesser T, Boellinghaus T (2013) Cold cracking tests – an overview of present technologies and applications. Weld World 57(1):3–37. https://doi.org/10.1007/s40194-012-0001-7

26. Kurji R, Coniglio N (2015) Towards the establishment of weldability test standards for hydrogen-assisted cold cracking. Int J Adv Manuf Technol 77(9–12):1581–1597. https://doi.org/10.1007/s00170-014-6555-3

27. Alexandrov B, Theis K, Streitenberger M, Herold H, Martinek I (2005) Cold cracking in weldments of steel S690QT. Weld World 49(5/6):64–73. https://doi.org/10.1007/BF03263411

28. Węglowski MS, Zeman M (2014) Prevention of cold cracking in ultra-high strength steel Weldox 1300. Arch Civ Mech Eng 14:417–424. https://doi.org/10.1016/j.acme.2013.10.010

29. Shiraiwa T, Kawate M, Brifford F, Kasuya T, Enoki M (2020) Evaluation of hydrogen-induced cracking in high-strength steel welded joints by acoustic emission technique. Mater Des 190:108573. https://doi.org/10.1016/j.matdes.2020.108573

30. Granjon HG (1969) The 'implants' method for studying the weldability of high strength steels. Met Constr-Brit Weld 1:509–515

31. Dickinson DW, Ries GD (1979) Implant testing of medium to high strength steel – a model for predicting delayed cracking susceptibility. Weld J 59(7):205s–211s

32. Sawhill JM, Dix AW, Savage WF (1974) Modified implant test for studying delayed cracking. Weld J 54(12):554s–560s

33. Saini N, Pandey C, Mahapatra MM (2017) Effect of diffusible hydrogen content on embrittlement of P92 steel. Int J Hydrog Energy 42:17328–17338. https://doi.org/10.1016/j.ijhydene.2017.05.214

34. Yadav U, Pandey C, Saini N, Thakre JG, Mahapatra MM (2017) Study on hydrogen-assisted cracking in high-strength steels by using the Granjon implant test. Metallogr Microstruct Anal 6(3):247–257. https://doi.org/10.1007/s13632-017-0351-z

35. Savage WF, Nippes EF, Sawhill JM (1976) Hydrogen induced cracking during implant testing of alloy steels. Weld J 56(12): 400s–407s

36. Yue X, Feng XL, Lippold JC (2013) Quantifying heat-affected zone hydrogen-induced cracking in high-strength naval steels. Weld J 92(9):265s–273s

37. Yue X (2015) Investigation on heat-affected zone hydrogen-induced cracking of high-strength naval steels using the Granjon implant test. Weld World 59(1):77–89. https://doi.org/10.1007/s40194-014-0181-4

38. ISO 3690 (2018) Welding and allied processes - determination of hydrogen content in arc weld metal

39. EN 10025–6 (2019) Hot rolled products of structural steels - part 6: technical delivery conditions for flat products of high yield strength structural steels in the quenched and tempered conditions

40. ISO 16834 (2012) Welding consumables - wire electrodes, wires, rods and deposits for gas shielded arc welding of high strength steels - classification

41. ISO 17642-3 (2005) Destructive tests on welds in metallic materials – cold cracking tests for weldments – Arc welding processes – Part 3: Externally loaded tests

42. ANSI/AWS B4.0 (2016) Standard methods for mechanical testing of welds. American Welding Society

43. Salmi S, Rhode M, Jüttner S, Zinke M (2015) Hydrogen determination in 22MnB5 steel grade by use of carrier gas hot extraction technique. Weld World 59(1):137–144. https://doi.org/10.1007/s40194-014-0186-z

44. Rhode M, Schaupp T, Muenster C, Mente T, Boellinghaus T, Kannengiesser T (2019) Hydrogen determination in welded specimens by carrier gas hot extraction—a review on the main parameters and their effects on hydrogen measurement. Weld World 63(2): 511–526. https://doi.org/10.1007/s40194-018-0664-9

45. ISO 14175 (2008) Welding consumables – gases and gas mixtures for fusion welding and allied processes

46. Kiefer JH (1996) Effects of moisture contamination and welding parameters on diffusible hydrogen. Weld J 75(5):155s–161s

47. Harwig DD, Longenecker DP, Cruz JH (1999) Effects of welding parameters and electrode atmospheric exposure on the diffusible hydrogen content of gas shielded flux cored arc welds. Weld J 78(9):314s–321s

48. Yahyaoui H (2020) Zur Bewertung der Kaltrissempfindlichkeit hochfester Feinkornbaustähle mittels Implant-Test beim Einsatz des modifizierten Sprühlichtbogens (Evaluation of HAC-susceptibility of high-strength structural steels by means of implant test using the modified spray arc). Unpublished masters thesis, University of Technology Berlin. (in German)

49. Schaupp T, Schroepfer D, Schroeder N, Kannengiesser T (2020) Modified TEKKEN test for studying hydrogen-assisted cracking in high-strength structural steels. IIW-Doc II-2157-2020

50. Schroepfer D, Kromm A, Schaupp T, Kannengiesser T (2019) Welding stress control in high-strength steel components using adapted heat control concepts. Weld World 63(3):647–661. https://doi.org/10.1007/s40194-018-00691-z

51. Dueren C (1986) Formulae for calculating the maximum hardness in the heat-affected zone of welded joints. IIW-Doc IX-1437-86

52. Stadtaus M (2014) FE-simulation der Verteilung von Wasserstoff und Stickstoff in Schweißverbindungen (numerical simulation of hydrogen and nitrogen distribution in welded joints). Dissertation, Shaker Verlag, Aachen. (in German)

53. Rhode M (2016) Hydrogen diffusion and effect on degradation in welded microstructures of creep-resistant low-alloyed steels. Dissertation, Otto-von-Guericke-University Magdeburg, BAM-Dissertationsreihe, Band 148. http://nbn-resolving.org/urn:nbn:de:kobv:b43-374027

54. ISO 18265 (2004) Metallic materials – conversion of hardness values

55. Beachem D (1972) A new model for hydrogen-assisted cracking (hydrogen «embrittlement»). Metall Mater Trans B 3(2):437–451. https://doi.org/10.1007/BF02642048

56. Gedeon SA, Eagar TW (1990) Assessing hydrogen-assisted cracking fracture modes in high-strength steel Weldments. Weld J 70(6): 213s–220s

57. Boellinghaus T, Hoffmeister H, Dangeleit A (1995) A scatterband for hydrogen diffusion coefficients in micro-alloyed and low carbon structural steels. Weld World 35(2):83–96

58. Rhode M, Richter T, Mayr P, Nitsche A, Mente T, Boellinghaus T (2020) Hydrogen diffusion in creep-resistant 9% Cr P91 multi-layer weld metal. Weld World 64:267–281. https://doi.org/10.1007/s40194-019-00828-8

59. Schroepfer D, Kromm A, Kannengiesser T (2017) Optimization of welding loads with narrow groove and application of modified spray arc process. Weld World 61:1077–1087. https://doi.org/10.1007/s40194-017-0484-3